

A modified projection approach to line mixing

Sven Nordebo*,

*Department of Physics and Electrical Engineering, Linnæus University, 351 95 Växjö, Sweden. E-mail: sven.nordebo@lnu.se

Abstract—This paper presents a simple approach to combine the high-resolution narrowband features of some desired isolated line models with the projection based strong collision (SC) method to line mixing which was introduced by Bulanin, Dokuchaev, Tonkov and Filippov. The method can be viewed in terms of a small diagonal perturbation of the SC relaxation matrix providing the required narrowband accuracy and resolution close to the line centers, at the same time as the SC line coupling transfer rates can be fine tuned to accurately match some given far wing absorption data. The method can conveniently be placed in the framework of the Boltzmann-Liouville transport equation where a rigorous diagonalization of the line mixing problem requires that molecular phase and velocity changes are assumed to be uncorrelated. Exact solutions and numerical examples are provided for the case with pure pressure broadening and velocity independent parameters. A detailed analysis for the general Doppler case is given based on the first order Rosenkranz approximation, including the possibility to incorporate quadratically speed dependent parameters such as with the Hartmann-Tran (HT) profile in the case with uncorrelated collisions.

Index Terms—Line mixing, wide-band molecular absorption spectra, spectral line shapes, Doppler broadening, collisional broadening, radiative transfer in the atmosphere.

I. INTRODUCTION

The presence of line mixing has been recognized as the main reason for the deviation of actual far wing line shapes from those that are calculated as a simple sum of Lorentzian lines, see *e.g.*, [1, Fig. 1] and [2, Fig. 2]. The effects of incomplete (soft) collisions does only play a minor role which motivates the use of the so called hard collision models within the impact approximation, see *e.g.*, [2], [3]. In this paper, we will investigate the possibility of complementing the high-resolution narrowband features of some desired isolated line models with the line coupling transfer rates obtained from the projection based strong collision (SC) method introduced in [1], [2], [4]–[7]. The aim is to derive a simple and flexible approach to line mixing with high accuracy close to the line centers as well as in the far wing. It is furthermore required that the spectral function should be implemented as a simple sum of individual lines based on a rigorous diagonalization of the line mixing problem.

The proposed approach can be motivated by the computationally exhaustive line-by-line calculations of broadband radiative transfer in the atmosphere, see *e.g.*, [8]–[10]. In particular, as may be quoted from Liou [8, p. 126]: “The computer time required for line-by-line calculations, even with the availability of a supercomputer, is formidable. This is especially true for flux calculations in which an integration over all absorption bands is necessary.” It is for this reason

that simple isolated line shapes are usually employed for this purpose, but it is quite unclear how much the lack of far wing accuracy and consequently the overestimated atmospheric absorption may affect the results. In this paper, we will focus on the derivation of a simple projection based approach to line mixing and which can use as sole input parameters the molecular transition frequencies, the line strengths and the line widths that are readily available for a large variety of species in spectroscopic databases such as *e.g.*, HITRAN [11]–[15].

We will take as a starting point the kinetic equation method by Rautian and Sobelman [3], [16]–[20] which can readily be adapted to include the line mixing effects as described in *e.g.*, [21]–[23]. There is a vast literature in this field, see *e.g.*, [3] with references, and among the pioneering work is in particular worth mentioning [24]–[28]. Later developments include the so called “beyond Voigt” profiles such as the Hartmann-Tran (HT) profile [19] encompassing partially correlated collisions and speed dependent pressure broadening and shifts, and which is now becoming standardized in spectroscopic databases such as HITRAN [20], [29]. However, following [23], it turns out that a rigorous diagonalization of the line mixing problem based on the kinetic equation method can only be achieved with uncorrelated collisions, line independent Dicke narrowing and speed independent pressure broadening and shifts, see in particular [23, Appendix A]. The more general line mixing methods may be computationally huge, *cf.*, *e.g.*, [23, p. 379] and [30, p. 73]. Nevertheless, it has been reported that the isolated HT line shapes can take line mixing effects into account by simple empirical modifications, *cf.*, *e.g.*, [19, Eq. (9)] and [30, Eq. (15)].

A simple projection based strong collision (SC) model for the relaxation matrix has previously been proposed in [1], [2], [4]–[7]. It has been reported that this model suffers from the major disadvantages that it does not take into account the distinguishing features of various perturbing gases nor of the different ro-vibrational branches of the radiator, see *e.g.*, [2, p. 131]. In particular, the model actually produces the same line width for all lines. However, as we will show in this paper, it will only require a small adjustment of this model based on a diagonal perturbation to obtain a line-mixing model that is able to take line specific data of various host gases and radiators into account and thus providing a high accuracy close to the line centers as well as in the far wing. The latter is achieved by fine tuning the one remaining model parameter (the collision frequency for line mixing) with respect to some given far wing measurement data. To this end, the perturbed matrix will retain the condition of detailed balancing, but its

property as a rigorous projector will be slightly relaxed in favor of the above mentioned new features.

Following [7, Eq. (10)-(12)] and [2, Eq. (14)-(15)], it is now possible to express explicitly an exact solution to the line mixing problem in the case of uncorrelated collisions, pure pressure broadening and velocity independent broadening and shifts parameters. To include Doppler broadening one can readily apply the first order Rosenkranz approximation. This will even allow the diagonal elements of the relaxation matrix to depend on speed, provided of course that the corresponding line shapes can be integrated in terms of the Faddeeva function, *cf.*, the HT profile with uncorrelated collisions [19], etc.

II. A STANDARD MODEL FOR LINE MIXING

As a standard hard collision line mixing model we consider here the following Boltzmann-Liouville transport equation formulated in velocity space as

$$\begin{aligned} \frac{\partial}{\partial t} F_n(\mathbf{v}, t) = & -i(\omega_{0n} + \mathbf{k} \cdot \mathbf{v}) F_n(\mathbf{v}, t) - \beta_n F_n(\mathbf{v}, t) \\ & + \beta_n f(\mathbf{v}) \int_{\mathbf{v}'} F_n(\mathbf{v}', t) d\mathbf{v}' - \sum_{n'=1}^N W_{nn'} F_{n'}(\mathbf{v}, t) \\ & - f(\mathbf{v}) \sum_{n'=1}^N C_{nn'} \int_{\mathbf{v}'} F_{n'}(\mathbf{v}', t) d\mathbf{v}', \quad (1) \end{aligned}$$

cf., [21]–[23], and where the notation has been largely adapted to [23]. Here, \mathbf{v} is the velocity, ω_{0n} is the transition frequency of a particular line n and the factor $\mathbf{k} \cdot \mathbf{v}$ models the Doppler dephasing where $\mathbf{k} = k\hat{\mathbf{k}}$ is the wave vector, $k = \omega/c_0$ the wavenumber of the incident radiation and c_0 the speed of light in vacuum. Further, $W_{nn'}$ are the relaxation coefficients for the phase-changing collisions which are uncorrelated with velocity changes and $C_{nn'}$ are the relaxation coefficients for the correlated phase-changing collisions which are simultaneously changing the velocity of the molecule. The parameters β_n are the line specific velocity-changing collision rates. The Maxwell-Boltzmann distribution is given by $f(\mathbf{v}) = (\sqrt{\pi}\tilde{v})^{-3} e^{-(v/\tilde{v})^2}$ where $v = |\mathbf{v}|$, $\tilde{v} = \sqrt{2k_B T/\mu_r}$ is the most probable speed, k_B the Boltzmann constant, T the temperature and μ_r the mass of the radiator. It is furthermore assumed here that the parameters $C_{nn'}$ and β_n are independent of velocity \mathbf{v} . The off-diagonal elements $W_{nn'}$ are the negative of the line coupling transfer rates and the diagonal elements $W_{nn} = \gamma_{0n}(v) + i\delta_{0n}(v)$ consists of the broadening and frequency shift parameters that generally may depend on speed. The parameters $W_{nn'}$, $C_{nn'}$ and β_n are typically taken to be linear with pressure p .

The total dipole autocorrelation function is represented here in velocity space as $C(t) = \int_{\mathbf{v}} C(\mathbf{v}, t) d\mathbf{v}$ where

$$C(\mathbf{v}, t) = \sum_n \mu_n F_n(\mathbf{v}, t), \quad (2)$$

and where μ_n are the transition dipole moments associated with a particular line. Based on the dipole approximation ($e^{-i\mathbf{k} \cdot \mathbf{r}} \approx 1$ where \mathbf{r} is the position of charges) the transition

dipole moments can be assumed here to be real valued. We have also

$$F_n(t) = \int_{\mathbf{v}} F_n(\mathbf{v}, t) d\mathbf{v}, \quad (3)$$

so that the total dipole autocorrelation function is given by

$$C(t) = \sum_n \mu_n F_n(t). \quad (4)$$

The initial condition in the hard collision model (1) is based on an assumption of thermal equilibrium at time zero, and is hence given by $F_n(\mathbf{v}, 0) = f(\mathbf{v})\rho_n\mu_n$ where ρ_n is the canonical (thermal equilibrium) density associated with the lower transition level of the unperturbed absorbing molecule. We have thus $F_n(0) = \rho_n\mu_n$ and we can now define the band strength as $C(0) = \sum_n S_n$ where $S_n = \rho_n\mu_n^2$ is the line strength. Finally, the condition of detailed balancing is assumed for the relaxation matrix so that $W_{kn}\rho_n = \rho_k W_{nk}$, *cf.*, [23].

We denote by $\tilde{C}(\omega) = \int_0^\infty C(t)e^{i\omega t} dt$ the Fourier-Laplace transform of the dipole autocorrelation function $C(t)$ having symmetry $C(-t) = C^*(t)$. The spectral density is then given by $I(\omega) = \frac{1}{2\pi} \int_{-\infty}^\infty C(t)e^{i\omega t} dt = \frac{1}{\pi} \text{Re}\{\tilde{C}(\omega)\}$ for $\omega \in \mathbb{R}$ where we are assuming that the real line belongs to the region of convergence of the corresponding Fourier-Laplace transform. Now, by using quantum mechanical principles, it can be shown that the absorption coefficient of a gaseous media, σ_a (in $\text{m}^2/\text{molecule}$), can be expressed quite generally (in SI-units) as¹

$$\sigma_a(\omega) = \frac{\pi\eta_0\omega}{3\hbar} (1 - e^{-\beta\hbar\omega}) I(\omega), \quad (5)$$

where $I(\omega)$ is the spectral density defined as above, ω the angular frequency, η_0 the wave impedance of vacuum, $\beta = 1/k_B T$ and $\hbar = h/2\pi$ where h is Planck's constant *cf.*, *e.g.*, [3, p. 12]. Here, the factor $1 - e^{-\beta\hbar\omega}$ above is due to the fluctuation-dissipation theorem stating that $I(-\omega) = e^{-\beta\hbar\omega} I(\omega)$, *cf.*, [3, p. 16]. It is finally noticed here that the frequency dependent parameter $k = \omega/c_0$ relating to the wavenumber of the incident radiation is present already in the time-domain in the expression (1) above.

A. Solving the line mixing problem

We will now formulate the solution to (1) based on various simplifying assumptions. In essence, this will follow the developments made in [23]. To simplify the notation we introduce a vector-matrix notation where $\mathbf{F}(\mathbf{v}, t)$ and $\boldsymbol{\mu}$ are column vectors with elements $F_n(\mathbf{v}, t)$ and μ_n , \mathbf{W} and \mathbf{C} are matrices with elements $W_{nn'}$ and $C_{nn'}$, and $\boldsymbol{\beta}$, $\boldsymbol{\omega}_0$ and $\boldsymbol{\rho}$ are the diagonal matrices $\boldsymbol{\beta} = \text{diag}\{\beta_n\}$, $\boldsymbol{\omega}_0 = \text{diag}\{\omega_{0n}\}$ and $\boldsymbol{\rho} = \text{diag}\{\rho_n\}$, respectively. The identity matrix is denoted \mathbf{I} . The line mixing

¹It may be noticed here that this formula is most often referred to in Gaussian units as $\sigma_a = \frac{4\pi^2\omega}{3\hbar c_0} I(\omega) (1 - e^{-\beta\hbar\omega})$, *cf.*, *e.g.*, [31, p. 3084], [32, p. 2348], [6, p. 111] and [3, p. 12].

problem (1) can now be formulated as the following initial value problem for $t \geq 0$

$$\begin{cases} \frac{\partial}{\partial t} \mathbf{F}(\mathbf{v}, t) = -(\mathbf{W} + \boldsymbol{\beta} + i(\boldsymbol{\omega}_0 + \mathbf{k} \cdot \mathbf{v} \cdot \mathbf{I})) \mathbf{F}(\mathbf{v}, t) \\ \quad + f(\mathbf{v}) (\boldsymbol{\beta} - \mathbf{C}) \int_{\mathbf{v}'} \mathbf{F}(\mathbf{v}', t) d\mathbf{v}' \\ \mathbf{F}(\mathbf{v}, 0) = f(\mathbf{v}) \boldsymbol{\rho} \boldsymbol{\mu}. \end{cases} \quad (6)$$

We define also the vector $\mathbf{F}(t)$ with elements $F_n(t)$, so that the correlation function can be expressed as $C(t) = \boldsymbol{\mu}^T \mathbf{F}(t)$ and its Fourier-Laplace transform as $\tilde{C}(\omega) = \boldsymbol{\mu}^T \tilde{\mathbf{F}}(\omega)$ where $\tilde{\mathbf{F}}(\omega)$ is the Fourier-Laplace transform of the vector $\mathbf{F}(t)$. From (3) we have also that $\tilde{\mathbf{F}}(\omega) = \int_{\mathbf{v}} \tilde{\mathbf{F}}(\mathbf{v}, \omega) d\mathbf{v}$ where $\tilde{\mathbf{F}}(\mathbf{v}, \omega)$ is the Fourier-Laplace transform of the vector $\mathbf{F}(\mathbf{v}, t)$.

We proceed now by taking the Fourier-Laplace transform of (6) yielding

$$\begin{aligned} -i\omega \tilde{\mathbf{F}}(\mathbf{v}, \omega) - f(\mathbf{v}) \boldsymbol{\rho} \boldsymbol{\mu} \\ = -(\mathbf{W} + \boldsymbol{\beta} + i(\boldsymbol{\omega}_0 + \mathbf{k} \cdot \mathbf{v} \cdot \mathbf{I})) \tilde{\mathbf{F}}(\mathbf{v}, \omega) \\ + f(\mathbf{v}) (\boldsymbol{\beta} - \mathbf{C}) \int_{\mathbf{v}'} \tilde{\mathbf{F}}(\mathbf{v}', \omega) d\mathbf{v}', \end{aligned} \quad (7)$$

or

$$\begin{aligned} (\mathbf{W} + \boldsymbol{\beta} - i(\boldsymbol{\omega} \cdot \mathbf{I} - \boldsymbol{\omega}_0 - \mathbf{k} \cdot \mathbf{v} \cdot \mathbf{I})) \tilde{\mathbf{F}}(\mathbf{v}, \omega) \\ - f(\mathbf{v}) (\boldsymbol{\beta} - \mathbf{C}) \int_{\mathbf{v}'} \tilde{\mathbf{F}}(\mathbf{v}', \omega) d\mathbf{v}' = f(\mathbf{v}) \boldsymbol{\rho} \boldsymbol{\mu}. \end{aligned} \quad (8)$$

Following the same procedure as in [23], we introduce now

$$\mathbf{G}(\mathbf{v}, \omega) = (\mathbf{W} + \boldsymbol{\beta} - i(\boldsymbol{\omega} \cdot \mathbf{I} - \boldsymbol{\omega}_0 - \mathbf{k} \cdot \mathbf{v} \cdot \mathbf{I}))^{-1}, \quad (9)$$

so that

$$\begin{aligned} \tilde{\mathbf{F}}(\mathbf{v}, \omega) - f(\mathbf{v}) \mathbf{G}(\mathbf{v}, \omega) (\boldsymbol{\beta} - \mathbf{C}) \int_{\mathbf{v}'} \tilde{\mathbf{F}}(\mathbf{v}', \omega) d\mathbf{v}' \\ = f(\mathbf{v}) \mathbf{G}(\mathbf{v}, \omega) \boldsymbol{\rho} \boldsymbol{\mu}. \end{aligned} \quad (10)$$

Next, by introducing

$$\mathbf{G}(\omega) = \int_{\mathbf{v}} f(\mathbf{v}) \mathbf{G}(\mathbf{v}, \omega) d\mathbf{v}, \quad (11)$$

and integrating (10) over velocity space, we obtain

$$\tilde{\mathbf{F}}(\omega) - \mathbf{G}(\omega) (\boldsymbol{\beta} - \mathbf{C}) \tilde{\mathbf{F}}(\omega) = \mathbf{G}(\omega) \boldsymbol{\rho} \boldsymbol{\mu}. \quad (12)$$

The solution to (12) can thus be expressed as

$$\tilde{\mathbf{F}}(\omega) = (\mathbf{I} - \mathbf{G}(\omega) (\boldsymbol{\beta} - \mathbf{C}))^{-1} \mathbf{G}(\omega) \boldsymbol{\rho} \boldsymbol{\mu}. \quad (13)$$

The Fourier-Laplace transform $\tilde{C}(\omega)$ is now given by

$$\begin{aligned} \tilde{C}(\omega) &= \boldsymbol{\mu}^T \tilde{\mathbf{F}}(\omega) \\ &= \boldsymbol{\mu}^T (\mathbf{I} - \mathbf{G}(\omega) (\boldsymbol{\beta} - \mathbf{C}))^{-1} \mathbf{G}(\omega) \boldsymbol{\rho} \boldsymbol{\mu}. \end{aligned} \quad (14)$$

This is the result given in [23, Eq. (2.13)].

In order to effectively exploit a diagonalization of the matrix $\mathbf{W} + \boldsymbol{\beta} + i\boldsymbol{\omega}_0$ and to write (14) as a sum over individual lines, we will see below that the eigenvectors of $\mathbf{W} + i\boldsymbol{\omega}_0$ must be independent of velocity (whereas its eigenvalues may depend on speed) and that $\boldsymbol{\beta} - \mathbf{C}$ must be proportional to

the identity matrix \mathbf{I} , *cf.*, also [23, Appendix A]. Hence, in the following we will assume that we have a case of Dicke narrowing with uncorrelated hard collisions where $\mathbf{C} = \mathbf{0}$ and $\boldsymbol{\beta} = \beta \mathbf{I}$ where β is the line-independent frequency of velocity changing collisions. We recall that the relaxation matrix \mathbf{W} satisfies the condition of detailed balancing, *i.e.*, $\mathbf{W} \boldsymbol{\rho} = \boldsymbol{\rho} \mathbf{W}^T$. We can then introduce the symmetric matrix $\boldsymbol{\Gamma} = \boldsymbol{\rho}^{-1/2} \mathbf{W} \boldsymbol{\rho}^{1/2}$ and start by diagonalizing the complex symmetric matrix

$$\boldsymbol{\Gamma} + i\boldsymbol{\omega}_0 = \mathbf{Q} \boldsymbol{\Lambda} \mathbf{Q}^T, \quad (15)$$

where $\boldsymbol{\Lambda}$ is a diagonal matrix of complex eigenvalues $\lambda_n = \gamma_n + i\omega_n$ and $\mathbf{Q}^{-1} = \mathbf{Q}^T$, *cf.*, [33, Theorem 4.4.13 on p. 211-212]. By pre- and post-multiplying (15) with $\boldsymbol{\rho}^{1/2}$ and $\boldsymbol{\rho}^{-1/2}$, respectively, we can readily see that

$$\mathbf{W} + i\boldsymbol{\omega}_0 = \mathbf{A} \boldsymbol{\Lambda} \mathbf{A}^{-1}, \quad (16)$$

where $\mathbf{A} = \boldsymbol{\rho}^{1/2} \mathbf{Q}$ and $\mathbf{A}^{-1} = \mathbf{Q}^T \boldsymbol{\rho}^{-1/2}$. We can also see that

$$\begin{aligned} \mathbf{W} + \beta \mathbf{I} - i(\boldsymbol{\omega} \cdot \mathbf{I} - \boldsymbol{\omega}_0 - \mathbf{k} \cdot \mathbf{v} \cdot \mathbf{I}) \\ = \mathbf{A} (\boldsymbol{\Lambda} + (\beta - i\boldsymbol{\omega} + i\mathbf{k} \cdot \mathbf{v}) \cdot \mathbf{I}) \mathbf{A}^{-1}, \end{aligned} \quad (17)$$

and hence diagonalize the expression (9) as

$$\begin{aligned} \mathbf{G}(\mathbf{v}, \omega) &= \mathbf{A} (\boldsymbol{\Lambda} + (\beta - i\boldsymbol{\omega} + i\mathbf{k} \cdot \mathbf{v}) \cdot \mathbf{I})^{-1} \mathbf{A}^{-1} \\ &= \mathbf{A} \cdot \text{diag} \left\{ \frac{1}{\gamma_n + \beta - i(\boldsymbol{\omega} - \boldsymbol{\omega}_n) + i\mathbf{k} \cdot \mathbf{v}} \right\} \mathbf{A}^{-1}. \end{aligned} \quad (18)$$

As already mentioned above, we will now assume that \mathbf{A} is independent of velocity. It follows then from (11) and (18) that

$$\mathbf{G}(\omega) = \int_{\mathbf{v}} f(\mathbf{v}) \mathbf{G}(\mathbf{v}, \omega) d\mathbf{v} = \mathbf{A} \mathbf{D}(\omega) \mathbf{A}^{-1}, \quad (19)$$

where

$$\begin{aligned} \mathbf{D}(\omega) &= \text{diag} \left\{ \int_{\mathbf{v}} \frac{f(\mathbf{v}) d\mathbf{v}}{\gamma_n + \beta - i(\boldsymbol{\omega} - \boldsymbol{\omega}_n) + i\mathbf{k} \cdot \mathbf{v}} \right\} \\ &= \text{diag} \left\{ \frac{\sqrt{\pi}}{k\tilde{v}} w \left(\frac{\boldsymbol{\omega} - \boldsymbol{\omega}_n + i(\gamma_n + \beta)}{k\tilde{v}} \right) \right\} \end{aligned} \quad (20)$$

and where the last line is valid when the eigenvalues λ_n are independent of velocity. Here, $w(z)$ denotes the Faddeeva function as defined in Appendix A and (78) has been used in the last step, *cf.*, also [23, p. 381].

Based on (14) with $\mathbf{C} = \mathbf{0}$ and $\boldsymbol{\beta} = \beta \mathbf{I}$ as well as the factorization (19), we can now write the final Fourier-Laplace transform as

$$\begin{aligned} \tilde{C}(\omega) &= \boldsymbol{\mu}^T (\mathbf{I} - \beta \mathbf{G}(\omega))^{-1} \mathbf{G}(\omega) \boldsymbol{\rho} \boldsymbol{\mu} \\ &= \boldsymbol{\mu}^T (\mathbf{A} \mathbf{I} \mathbf{A}^{-1} - \beta \mathbf{A} \mathbf{D}(\omega) \mathbf{A}^{-1})^{-1} \mathbf{A} \mathbf{D}(\omega) \mathbf{A}^{-1} \boldsymbol{\rho} \boldsymbol{\mu} \\ &= \boldsymbol{\mu}^T \mathbf{A} (\mathbf{I} - \beta \mathbf{D}(\omega))^{-1} \mathbf{D}(\omega) \mathbf{A}^{-1} \boldsymbol{\rho} \boldsymbol{\mu} \\ &= \boldsymbol{\mu}^T \boldsymbol{\rho}^{1/2} \mathbf{Q} (\mathbf{I} - \beta \mathbf{D}(\omega))^{-1} \mathbf{D}(\omega) \mathbf{Q}^T \boldsymbol{\rho}^{-1/2} \boldsymbol{\rho} \boldsymbol{\mu} \\ &= \mathbf{M}^T \mathbf{Q} (\mathbf{I} - \beta \mathbf{D}(\omega))^{-1} \mathbf{D}(\omega) \mathbf{Q}^T \mathbf{M}, \end{aligned} \quad (21)$$

where $\mathbf{A} = \boldsymbol{\rho}^{1/2} \mathbf{Q}$, $\mathbf{A}^{-1} = \mathbf{Q}^T \boldsymbol{\rho}^{-1/2}$ and $\mathbf{M} = \boldsymbol{\rho}^{1/2} \boldsymbol{\mu}$. Let us now just briefly return to the general case (14) and

realize that the factorization $\mathbf{G}(\omega) = \mathbf{A}\mathbf{D}(\omega)\mathbf{A}^{-1}$ does not help diagonalize the final expression (21) unless the matrices \mathbf{A}^{-1} and $\beta - \mathbf{C}$ commute, *cf.*, [23, Appendix A]. We can also see in the simplified analysis above why it is essential that \mathbf{A} is independent of velocity. Thus, coming back to our special case with uncorrelated Dicke narrowing where $\beta - \mathbf{C} = \beta\mathbf{I}$ as in (21) above, we can now see that $\tilde{C}(\omega)$ can be written as the following sum over individual lines

$$\tilde{C}(\omega) = \sum_n \frac{a_n^2 D_n(\omega)}{1 - \beta D_n(\omega)}, \quad (22)$$

where $D_n(\omega)$ are the diagonal elements defined by (20), and

$$a_n = \mathbf{M}^T \mathbf{q}_n \quad (23)$$

where \mathbf{q}_n is the n th column of \mathbf{Q} .

The effect of Doppler broadening can be ignored by putting the wave number $k = 0$ while keeping ω fixed, which immediately yields

$$D_n(\omega) = \frac{1}{\gamma_n + \beta - i(\omega - \omega_n)}, \quad (24)$$

provided that the eigenvalues $\lambda_n = \gamma_n + i\omega_n$ are independent of velocity. However, in this case we can readily see that the solution becomes independent of β , and hence

$$\tilde{C}(\omega) = \sum_n \frac{a_n^2}{\gamma_n - i(\omega - \omega_n)}. \quad (25)$$

In fact, we can readily see already in (8) that the solution will be independent of β when $\mathbf{k} = \mathbf{0}$. Physically, this means that the frequency of velocity changing collisions are of no significance if there is no Doppler effect ($k = 0$) and that Dicke narrowing is a pure Doppler phenomena [16].

B. Rosenkranz parameters

We consider now the spectral decomposition (15), or equivalently (16) where $\mathbf{\Gamma} = \boldsymbol{\rho}^{-1/2} \mathbf{W} \boldsymbol{\rho}^{1/2}$. We recall that $(\mathbf{\Gamma} + i\omega_0) \mathbf{q}_n = \lambda_n \mathbf{q}_n$ and $\lambda_n = \gamma_n + i\omega_n$. Assuming that $\mathbf{\Gamma} = p\hat{\mathbf{\Gamma}}$ where p is pressure, the Rosenkranz parameters are given by the following first order approximations

$$\lambda_n = p\hat{\Gamma}_{nn} + i\omega_{0n}, \quad (26)$$

and

$$q_{kn} = \begin{cases} 1 & k = n \\ \frac{ip\hat{\Gamma}_{kn}}{\omega_{0k} - \omega_{0n}} & k \neq n, \end{cases} \quad (27)$$

where q_{kn} are the elements of \mathbf{q}_n , *cf.*, [28, (A.4) and (A.5)]. It is noted that this analysis can be performed already in velocity space if the eigenvalues λ_n depend on \mathbf{v} . Based on (23) and (27), we can now find that

$$a_n = M_n + ip \sum_{k \neq n} M_k \frac{\hat{\Gamma}_{kn}}{\omega_{0k} - \omega_{0n}} \quad (28)$$

and to first order in p we can also derive the following expression

$$\begin{aligned} a_n^2 &= M_n^2 + 2ipM_n \sum_{k \neq n} \frac{M_k \hat{\Gamma}_{kn}}{\omega_{0k} - \omega_{0n}} \\ &= \rho_n \mu_n^2 + 2ip\rho_n \mu_n \sum_{k \neq n} \frac{\mu_k \hat{W}_{kn}}{\omega_{0k} - \omega_{0n}}, \end{aligned} \quad (29)$$

where we have also employed the definitions $M_n = \rho_n^{1/2} \mu_n$ and $\hat{\Gamma}_{kn} = \rho_k^{-1/2} \hat{W}_{kn} \rho_n^{1/2}$, *cf.*, [28, Eq. (2) and (3)].

III. A MODIFIED PROJECTION BASED MODEL FOR LINE MIXING

A simple projection based strong collision model for the relaxation matrix \mathbf{W} has previously been proposed in [1], [2], [4]–[7]. The determination of this matrix requires no additional spectral parameters except for the (theoretical or experimental) center frequencies ω_{0n} , the transition dipole moments μ_n , the molecular canonical densities ρ_n and the line widths γ_{0n} of the individual lines. Here, the line strengths are furthermore given by $S_n = M_n^2$ where $M_n = \rho_n^{1/2} \mu_n$. It has previously been reported that this model suffers from the major disadvantage that it does not take into account the distinguishing features of various perturbing gases nor of the different ro-vibrational branches of the radiator, *cf.*, [2]. The model also produces the same line width for all lines. However, as we will show below, it will only require a small adjustment of this model based on a diagonal perturbation to obtain a line-mixing model that is able to take into account line specific data relating to various perturbing gases. The one remaining model parameter v_s (collision frequency for line mixing) can furthermore be adjusted empirically to the particular radiator and host being used. A major advantage of this line mixing model is that the computation of line shapes as in (22) will only require the prior knowledge of individual center frequencies ω_{0n} , line widths γ_{0n} and line strengths S_n , in addition to the parameter v_s to be discussed below.

A. The basic projection based method

The basic projection based strong collision (SC) method has been proposed in *e.g.*, [1], [2], [4]–[7] and is briefly summarized below. Within this strong collision model it is assumed that the relaxation time τ_s is equal to the mean duration between successive collisions for any rotational state of the absorbing molecule [6]. It is furthermore assumed that $\omega_{0n}\tau_s \ll 1$, and the corresponding collision frequency is defined as $v_s = \tau_s^{-1}$. The symmetrized relaxation matrix $\mathbf{\Gamma}$ can now be defined in terms of a projector $\mathbf{I} - \tau_s \mathbf{\Gamma}$ that restores thermal equilibrium at the characteristic time τ_s , and hence

$$\mathbf{\Gamma} = v_s \left(\mathbf{I} - \frac{\mathbf{M}\mathbf{M}^T}{\mathbf{M}^T\mathbf{M}} \right), \quad (30)$$

where $\mathbf{M} = \boldsymbol{\rho}^{1/2} \boldsymbol{\mu}$, *cf.*, *e.g.*, [2, Eq. (13)] and [6]. The corresponding unsymmetric relaxation matrix is then given by

$$\mathbf{W} = \boldsymbol{\rho}^{1/2} \mathbf{\Gamma} \boldsymbol{\rho}^{-1/2} = v_s \left(\mathbf{I} - \frac{\boldsymbol{\rho} \boldsymbol{\mu} \boldsymbol{\mu}^T}{\boldsymbol{\mu}^T \boldsymbol{\rho} \boldsymbol{\mu}} \right), \quad (31)$$

and which thus satisfies the condition of detailed balancing $\mathbf{W}\boldsymbol{\rho} = \boldsymbol{\rho}\mathbf{W}^T$. It is also noticed here that $C(0) = \boldsymbol{\mu}^T \boldsymbol{\rho} \boldsymbol{\mu} = \mathbf{M}^T \mathbf{M}$.

The line width parameter v_s can now be chosen so that the theoretical or experimental line widths γ_{0n} are suitably approximated by the diagonal elements $W_{nn} = \Gamma_{nn} = v_s(1 - S_n/C(0))$. To this end, the following formula

$$v_s = \frac{\sum_n \gamma_{0n} S_n}{\sum_n S_n}, \quad (32)$$

has been suggested in *e.g.*, [6, p. 113] and [2, Eq. (16)].

The strong collision (SC) model above has been validated against experimental data and compared to an improved technique referred to as adjustable branch coupling (ABC) in *e.g.*, [2], [7]. It has been demonstrated that both the SC and ABC methods are able to provide significantly better predictions of the far wing behavior of an absorbing gas in comparison to a simple sum of isolated Lorentzian lines. The ABC method is however more sophisticated as it requires the subdivision of lines into isolated branches, but it is also able to provide better predictions as it employs one additional free parameter (interbranch interaction) to match the model to experimental data. In our approach here we wish to retain the simplicity of the SC projection method to line coupling described above, while at the same time reinstalling the high-resolution aspects of some standard isolated line models. This will be the topic of the sections to follow.

B. Perturbation

We will now aim to improve the simple strong collision (SC) projection method above by introducing the slightly perturbed model

$$\Gamma_{kn} = \begin{cases} \gamma_{0n}(v) + i\delta_{0n}(v) & k = n, \\ -v_s \frac{M_k M_n}{C(0)} & k \neq n, \end{cases} \quad (33)$$

where the diagonal elements in (30) have been replaced by any (theoretical or experimental) presumably more accurate and possibly even speed dependent broadening and shift parameters $\gamma_{0n}(v) + i\delta_{0n}(v)$. The same off-diagonal elements as in (30) are retained as a model of the line coupling transfer rates. However, the parameter v_s will now be treated as an empirical parameter that can readily be adjusted to match experimental data. It is noted that the unsymmetric relaxation matrix $\mathbf{W} = \boldsymbol{\rho}^{1/2} \boldsymbol{\Gamma} \boldsymbol{\rho}^{-1/2}$ is still satisfying the condition of detailed balance, just as before.

The modification introduced in (33) means that we have now added to (30) the diagonal perturbation matrix

$$\mathbf{P} = \text{diag}\{\gamma_{0n} + i\delta_{0n} - v_s(1 - S_n/C(0))\}, \quad (34)$$

and consequently the perturbed matrix (33) does no longer correspond to a rigorous projector. However, the perturbed model does provide a useful compromise in the sense that the rigorous projector is only slightly relaxed in favor of providing

two new features: An accurate modeling close to the line centers as well as an accurate modeling in the far wings, the latter being achieved by fine tuning the parameter v_s .

Let us now briefly discuss the properties of the two orthogonal projectors $\mathbf{I} - \tau_s \boldsymbol{\Gamma}$ and $\tau_s \boldsymbol{\Gamma}$, the former ideally being a projector onto the space parallel to \mathbf{M} and the latter orthogonal to \mathbf{M} . Let us now consider a vector $\mathbf{x} = \mathbf{x}_{\parallel} + \mathbf{x}_{\perp}$ being correspondingly represented in line space, and where

$$(\mathbf{I} - \tau_s \boldsymbol{\Gamma}) \mathbf{x} = \mathbf{x}_{\parallel} + (\mathbf{I} - \tau_s \boldsymbol{\Gamma}) \mathbf{x}_{\perp} - \tau_s \boldsymbol{\Gamma} \mathbf{x}_{\parallel}. \quad (35)$$

The first term on the right-hand side of (35) is what we aim for. It is now assumed that the state of the system under consideration which is involving molecular collisions is always relatively close to thermal equilibrium, and hence that the vector \mathbf{x}_{\parallel} is dominant over the vector \mathbf{x}_{\perp} . The perturbed matrix $\mathbf{I} - \tau_s \boldsymbol{\Gamma}$ is furthermore an approximate projector almost orthogonal to \mathbf{x}_{\perp} , all of which now makes the second term negligible. Hence, it is the vanishing of the last term in (35) that is the most important for maintaining the required projection property. To this end, it is noted that the required orthogonality property $\boldsymbol{\Gamma} \mathbf{M} = \mathbf{0}$ is also referred to as a sum rule in [6, p. 113] and [2, Eq. (4)]. In the present context this means that we should now choose the parameter v_s to minimize the least squares norm of the vector $\mathbf{P} \mathbf{M}$, yielding

$$v_s^{\text{ls}} = \frac{\sum_n \gamma_{0n} S_n \left(1 - \frac{S_n}{C(0)}\right)}{\sum_n S_n \left(1 - \frac{S_n}{C(0)}\right)^2}, \quad (36)$$

where $C(0) = \sum_n S_n$. It may be noticed that the expression (36) also corresponds to an S_n -weighted least squares solution to minimize the error $v_s(1 - S_n/C(0)) - \gamma_{0n}$ related to (30), and that (32) is obtained if the ratio $S_n/C(0)$ can be neglected. Notably, if γ_{0n} is a speed dependent parameter, we would use in (36) either an average $\bar{\gamma}_{0n} = \int_v f(v) \gamma_{0n} dv$, or we would evaluate γ_{0n} at the most probable speed \tilde{v} to obtain a speed independent parameter v_s .

In practice, we have found that it is very useful to make a very small fine tuning of (36) to slightly increase the line coupling transfer rates for a better match to measurement data. Hence, we may choose $v_s = c v_s^{\text{ls}}$ where c is a constant very close to 1 ($c = 1.005$ in our numerical examples for CO_2 in the ν_3 -band). This fine tuning of v_s has insignificant effect on the absorption close to the line centers, but it can provide an appropriate correction of the far wing behavior. Obviously, the parameter c can readily be adjusted to match the experimental data of any specific species and ro-vibrational bands of interest.

C. Rosenkranz parameters

Since the matrix \mathbf{W} is assumed to be linear with pressure p and $\boldsymbol{\Gamma} = p \hat{\boldsymbol{\Gamma}}$, we introduce now also the notation $\gamma_{0n} + i\delta_{0n} = p(\hat{\gamma}_{0n} + i\hat{\delta}_{0n})$ and $v_s = p \hat{v}_s$. By following (26) through

(29) and to the first order in p , the corresponding Rosenkranz parameters are now obtained as

$$\begin{cases} \gamma_n = p\widehat{\gamma}_{0n}, \\ \omega_n = \omega_{0n} + p\widehat{\delta}_{0n}, \end{cases} \quad (37)$$

as well as

$$a_n = M_n + \frac{ip\widehat{v}_s M_n}{C(0)} \sum_{k \neq n} \frac{S_k}{\omega_{0n} - \omega_{0k}} \quad (38)$$

and

$$a_n^2 = M_n^2 + \frac{2ip\widehat{v}_s M_n^2}{C(0)} \sum_{k \neq n} \frac{S_k}{\omega_{0n} - \omega_{0k}}. \quad (39)$$

It is finally noted that the only prior knowledge required for the computation of (37), (38) and (39) (except for the design parameter $c \approx 1$ where $\widehat{v}_s = c\widehat{v}_s^{\text{ls}}$) are the center frequencies ω_{0n} , the line widths γ_{0n} and the line strengths S_n . These are parameters that are readily available for a large variety of species in spectroscopic databases such as *e.g.*, HITRAN [11]–[15].

D. Exact solution

Following the ideas presented in [7, Eq. (10)–(12)] and [2, Eq. (14)–(15)], it is possible to develop a simple closed form solution to (6) for the case with uncorrelated collisions without velocity changes and where $\mathbf{\Gamma}$ is given by the modified projection model (33). Hence, in this case we have $\mathbf{C} = \mathbf{0}$ and $\boldsymbol{\beta} = \mathbf{0}$, and (9) and (10) yield

$$\begin{aligned} \widetilde{C}(\mathbf{v}, \omega) &= \boldsymbol{\mu}^T \widetilde{\mathbf{F}}(\mathbf{v}, \omega) \\ &= \boldsymbol{\mu}^T (\mathbf{W} - i(\omega \cdot \mathbf{I} - \omega_0 - \mathbf{k} \cdot \mathbf{v} \cdot \mathbf{I}))^{-1} f(\mathbf{v}) \boldsymbol{\rho} \boldsymbol{\mu}. \end{aligned} \quad (40)$$

By employing $\mathbf{W} = \boldsymbol{\rho}^{1/2} \mathbf{\Gamma} \boldsymbol{\rho}^{-1/2}$ and $\mathbf{M} = \boldsymbol{\rho}^{1/2} \boldsymbol{\mu}$ we obtain the symmetrized form

$$\widetilde{C}(\mathbf{v}, \omega) = \mathbf{M}^T (\mathbf{\Gamma} - i(\omega \cdot \mathbf{I} - \omega_0 - \mathbf{k} \cdot \mathbf{v} \cdot \mathbf{I}))^{-1} \mathbf{M} f(\mathbf{v}), \quad (41)$$

and by inserting (33) we obtain

$$\begin{aligned} \widetilde{C}(\mathbf{v}, \omega) &= \mathbf{M}^T \left(\mathbf{P} + v_s \left(\mathbf{I} - \frac{\mathbf{M} \mathbf{M}^T}{C(0)} \right) \right. \\ &\quad \left. - i(\omega \cdot \mathbf{I} - \omega_0 - \mathbf{k} \cdot \mathbf{v} \cdot \mathbf{I}) \right)^{-1} \mathbf{M} f(\mathbf{v}), \end{aligned} \quad (42)$$

where $\mathbf{P} = \text{diag}\{\gamma_{0n} + i\delta_{0n} - v_s(1 - S_n/C(0))\}$. Now, we introduce the matrices

$$\mathbf{D}^{-1} = \text{diag} \left\{ \gamma_{0n} + i\delta_{0n} + v_s \frac{S_n}{C(0)} - i(\omega - \omega_{0n} - \mathbf{k} \cdot \mathbf{v}) \right\}, \quad (43)$$

and

$$\mathbf{E}^{-1} = -\frac{v_s}{C(0)} \quad (44)$$

and write

$$\widetilde{C}(\mathbf{v}, \omega) = \mathbf{M}^T (\mathbf{D}^{-1} + \mathbf{M} \mathbf{E}^{-1} \mathbf{M}^T)^{-1} \mathbf{M} f(\mathbf{v}). \quad (45)$$

By making use of the so called matrix inversion lemma [34, p. 30], it can readily be seen that the exact solution in velocity space is given by

$$\begin{aligned} \widetilde{C}(\mathbf{v}, \omega) &= \mathbf{M}^T \left(\mathbf{D} - \mathbf{D} \mathbf{M} (\mathbf{M}^T \mathbf{D} \mathbf{M} + \mathbf{E})^{-1} \mathbf{M}^T \mathbf{D} \right) \mathbf{M} f(\mathbf{v}). \end{aligned} \quad (46)$$

After some algebra, it is found that

$$\widetilde{C}(\mathbf{v}, \omega) = \frac{\mathbf{M}^T \mathbf{D} \mathbf{M} f(\mathbf{v})}{1 + \mathbf{E}^{-1} \mathbf{M}^T \mathbf{D} \mathbf{M}} = \frac{\widetilde{C}_1(\mathbf{v}, \omega) f(\mathbf{v})}{1 - \frac{v_s}{C(0)} \widetilde{C}_1(\mathbf{v}, \omega)} \quad (47)$$

where

$$\begin{aligned} \widetilde{C}_1(\mathbf{v}, \omega) &= \mathbf{M}^T \mathbf{D} \mathbf{M} \\ &= \sum_n \frac{S_n}{\gamma_{0n} + v_s \frac{S_n}{C(0)} - i(\omega - \omega_{0n} - \delta_{0n} - \mathbf{k} \cdot \mathbf{v})}, \end{aligned} \quad (48)$$

and where $S_n = M_n^2$ and $C(0) = \sum_n S_n$. The total Fourier-Laplace transform $\widetilde{C}(\omega)$ is finally obtained by integrating over velocity space as

$$\widetilde{C}(\omega) = \int_{\mathbf{v}} \widetilde{C}(\mathbf{v}, \omega) d\mathbf{v}. \quad (49)$$

In the case when the Doppler effect can be neglected we can set $k = 0$ in (48), and if the broadening and shift parameters $\gamma_{0n} + i\delta_{0n}$ are furthermore independent of velocity then (47) gives after integration

$$\widetilde{C}(\omega) = \frac{\widetilde{C}_1(\omega)}{1 - \frac{v_s}{C(0)} \widetilde{C}_1(\omega)} \quad (50)$$

where

$$\widetilde{C}_1(\omega) = \sum_n \frac{S_n}{\gamma_{0n} + v_s \frac{S_n}{C(0)} - i(\omega - \omega_{0n} - \delta_{0n})}. \quad (51)$$

Unfortunately, the function (47) can not readily be integrated over velocity space based on (48) when Doppler broadening is present and $k \neq 0$. However, if we can assume that the Boltzmann factor $e^{-(v/\widehat{v})^2}$ is very narrow in comparison to the variations in $\widetilde{C}_1(\mathbf{v}, \omega)$, *i.e.*, if $k\widehat{v}/\gamma_{0n} \ll 1$, then we may approximate (49) by applying the $f(\mathbf{v})$ -weighted integration (averaging) separately to the numerator and the denominator of (47), respectively. Assuming once again that $\gamma_{0n} + i\delta_{0n}$ are independent of velocity this will then yield a result of the same form as in (50) where

$$\begin{aligned} \widetilde{C}_1(\omega) &= \int_{\mathbf{v}} \widetilde{C}_1(\mathbf{v}, \omega) f(\mathbf{v}) d\mathbf{v} \\ &= \frac{\sqrt{\pi}}{k\widehat{v}} \sum_n S_n w \left(\frac{\omega - \omega_{0n} - \delta_{0n} + i \left(\gamma_{0n} + v_s \frac{S_n}{C(0)} \right)}{k\widehat{v}} \right) \end{aligned} \quad (52)$$

and where $w(\cdot)$ is the Faddeeva function based on the integral identity (78). Eventhough (52) does not provide a rigorous calculation of (49), it is similar to the results obtained in

[1, Eq. (9)], and it has the correct asymptotics as $k \rightarrow 0$ in accordance with (51). However, perhaps a more rigorous alternative for including the Doppler effect is then to employ the diagonalization (20) and (22) together with the Rosenkranz parameters (37) and (38), and which is also providing the option to include Dicke narrowing with parameter β .

IV. WAVENUMBER DOMAIN

A. Parameter scalings

We summarize the results of this section by transforming the expressions to the wavenumber domain via the substitution $\omega = 2\pi c_0 \nu$ where $\nu = \lambda^{-1}$ is the wavenumber and λ the wavelength of the radiation. We have thus $I(\nu) = 2\pi c_0 I(\omega)$ and

$$\int I(\omega) d\omega = \int I(\nu) d\nu = C(0) = \sum_n S_n, \quad (53)$$

where the correlation function $C(t)$ as well as the line strengths S_n are invariant to the substitution. The corresponding Fourier-Laplace transform is similarly defined so that $\tilde{C}(\nu) = 2\pi c_0 \tilde{C}(\omega)$ and $I(\nu) = \frac{1}{\pi} \text{Re}\{\tilde{C}(\nu)\}$.

Now, we have seen previously in (5) that the absorption coefficient can be expressed as $\sigma_a = \frac{\pi \eta_0 \omega}{3\hbar} (1 - e^{-\beta \hbar \omega}) I(\omega)$ where $I(\omega) = \frac{1}{2\pi} \int_{-\infty}^{\infty} C(t) e^{i\omega t} dt$ is the Fourier transform of the dipole autocorrelation function $C(t)$. However, since the factor $\omega(1 - e^{-\beta \hbar \omega})$ is only slowly varying over a typical ro-vibrational band, the absorption coefficient σ_a can be approximated as being proportional to $I(\omega)$. Here, we will assume that $\sigma_a = I(\nu)$ as is customary with spectroscopic data bases such as *e.g.*, HITRAN [11]–[15]. This means that the correlation function $C(t)$ as well as the line strengths S_n are now suitable scaled to have length dimensions and $I(\nu)$ is given in area units.

We introduce now the following parameter scaling

$$[\gamma_{0n}, \delta_{0n}, \gamma_n, v_s, \beta, \gamma_D] = 2\pi c_0 [\gamma'_{0n}, \delta'_{0n}, \gamma'_n, v'_s, \beta', \gamma'_D], \quad (54)$$

where the unprimed parameters refer to the frequency domain and the primed parameters to the wavenumber domain. Here, we are furthermore introducing the Doppler half-width parameter $\gamma_D = k\tilde{v}\sqrt{\ln 2}$ so that

$$\gamma'_D = \frac{\nu \tilde{v} \sqrt{\ln 2}}{c_0}, \quad (55)$$

where $k = 2\pi\nu$. For notational convenience it is also natural to write $\omega_{0n} = 2\pi c_0 \nu_{0n}$ and $\omega_n = 2\pi c_0 \nu_n$. The Fourier-Laplace transform in (22) now becomes

$$\tilde{C}(\nu) = \sum_n \frac{a_n^2 D_n(\nu)}{1 - \beta' D_n(\nu)}, \quad (56)$$

where

$$\begin{aligned} D_n(\nu) &= 2\pi c_0 D_n(\omega) \\ &= \int_{\mathbf{v}} \frac{f(\mathbf{v}) d\mathbf{v}}{\gamma'_n + \beta' - i(\nu - \nu_n) + i \frac{\gamma'_D}{\tilde{v}\sqrt{\ln 2}} \hat{\mathbf{k}} \cdot \mathbf{v}} \\ &= \frac{\sqrt{\pi}}{\gamma'_D / \sqrt{\ln 2}} w \left(\frac{\nu - \nu_n + i(\gamma'_n + \beta')}{\gamma'_D / \sqrt{\ln 2}} \right), \end{aligned} \quad (57)$$

and where the last line is valid when the eigenvalues $\lambda'_n = \gamma'_n + i\nu_n$ are independent of velocity, *cf.*, (20). Without Doppler broadening for $k = 0$, we employ instead (24) to yield

$$D_n(\nu) = \frac{1}{\gamma'_n + \beta' - i(\nu - \nu_n)}, \quad (58)$$

where β' is again redundant as in (25), yielding

$$\tilde{C}(\nu) = \sum_n \frac{a_n^2}{\gamma'_n - i(\nu - \nu_n)}. \quad (59)$$

We can see from the definition made in (23) that the parameter $a_n = \mathbf{M}^T \mathbf{q}_n$ used in (56) and (59) is invariant under the substitution $\omega = 2\pi c_0 \nu$. In particular, the spectral decomposition $\mathbf{\Gamma} + i\omega_0 = \mathbf{Q} \mathbf{\Lambda} \mathbf{Q}^T$ which was defined in (15) now becomes $\mathbf{\Gamma}' + i\nu_0 = \mathbf{Q} \mathbf{\Lambda}' \mathbf{Q}^T$ where $\mathbf{\Gamma}' = \mathbf{\Gamma} / 2\pi c_0$, $\nu_0 = \text{diag}\{\nu_{0n}\}$ and $\lambda'_n = \lambda_n / 2\pi c_0 = \gamma'_n + i\nu_n$. Thus, the eigenvalues λ_n are scaled as the frequency parameters, but the eigenvectors \mathbf{q}_n are dimensionfree invariants. However, since $I(\nu)$ is now given in area units, the parameter a_n^2 must be given in length dimension just like S_n and $\mathbf{M} = \rho^{1/2} \boldsymbol{\mu}$ in square root of length, just like $\boldsymbol{\mu}$.

The modified projection method based on the perturbed relaxation matrix (33) is now given by

$$\Gamma'_{kn} = \begin{cases} \gamma'_{0n}(v) + i\delta'_{0n}(v) & k = n, \\ -v'_s \frac{M_k M_n}{C(0)} & k \neq n, \end{cases} \quad (60)$$

and where $\gamma'_{0n} + i\delta'_{0n} = p(\hat{\gamma}'_{0n} + i\hat{\delta}'_{0n})$ and $v'_s = p\hat{v}'_s$ where p is pressure. Assuming that the broadening and shift parameters $\gamma'_{0n} + i\delta'_{0n}$ are furthermore independent of velocity, the design parameter \hat{v}'_s can initially be chosen as in (36), which becomes

$$\hat{v}'_s = \frac{\sum_n \hat{\gamma}'_{0n} S_n \left(1 - \frac{S_n}{C(0)}\right)}{\sum_n S_n \left(1 - \frac{S_n}{C(0)}\right)^2}, \quad (61)$$

where $C(0) = \sum_n S_n$ and $M_n = \sqrt{S_n}$. In order to fine tune the far wing accuracy of model the parameter \hat{v}'_s can now be chosen as $\hat{v}'_s = c\hat{v}'_s$ where c is a constant very close to one.

B. Rosenkranz parameters

The general first order Rosenkranz parameters are now obtained from (26) through (28) as

$$\lambda'_{nn} = p\hat{\Gamma}'_{nn} + i\nu_{0n}, \quad (62)$$

as well as

$$a_n = M_n + ip \sum_{k \neq n} M_k \frac{\hat{\Gamma}'_{kn}}{\nu_{0k} - \nu_{0n}} \quad (63)$$

where $\hat{\Gamma}'_{kn} = \hat{\Gamma}_{kn}/2\pi c_0$. The corresponding Rozenkranz parameters based on the modified projection method (33) are given by (37) and (38) and which transforms to the wavenumber domain as

$$\begin{cases} \gamma'_n = p\hat{\gamma}'_{0n}, \\ \nu_n = \nu_{0n} + p\hat{\delta}'_{0n}, \end{cases} \quad (64)$$

and

$$a_n = M_n + \frac{ip\hat{\nu}'_s M_n}{C(0)} \sum_{k \neq n} \frac{S_k}{\nu_{0n} - \nu_{0k}}. \quad (65)$$

C. Exact solution

In the case when there is no Doppler broadening ($k = 0$) and if the broadening and shift parameters $\gamma'_{0n} + i\delta'_{0n}$ are furthermore independent of velocity then the exact solution in (50) and (51) becomes

$$\tilde{C}(\nu) = \frac{\tilde{C}_1(\nu)}{1 - \frac{\nu'_s}{C(0)} \tilde{C}_1(\nu)} \quad (66)$$

where

$$\tilde{C}_1(\nu) = \sum_n \frac{S_n}{\gamma'_{0n} + \nu'_s \frac{S_n}{C(0)} - i(\nu - \nu_{0n} - \delta'_{0n})}. \quad (67)$$

Similar expressions can be derived with regard to (52).

D. Basic projection method

As for a comparison, based on the original unperturbed strong collision model (30), we will use instead

$$\tilde{\nu}'_s = \frac{\sum_n \tilde{\gamma}'_{0n} S_n}{\sum_n S_n}, \quad (68)$$

and in the case with no Doppler broadening ($k = 0$) and an exact solution, we will employ (66) together with

$$\tilde{C}_1(\nu) = \sum_n \frac{S_n}{\nu'_s - i(\nu - \nu_{0n})}, \quad (69)$$

as suggested in [7, Eq. (10)-(12)] and [2, Eq. (14)-(15)]. As for the Rosenkranz approximation based on the unperturbed model (30), the only difference is with the computation of eigenvalues where

$$\begin{cases} \gamma'_n = p\tilde{\nu}'_s(1 - S_n/C(0)), \\ \nu_n = \nu_{0n}, \end{cases} \quad (70)$$

instead of (64). The other relations (56) through (59) and (65) are obtained as above.

V. NUMERICAL EXAMPLES

In Figs. 1 through 3 are shown the relative absorption coefficients for the ν_3 CO₂-band in dry air at $T = 20^\circ\text{C}$ and total pressure $p = 1$ atm, calculated using HITRAN2016 parameters [15]. The input parameters γ_{0n} and δ_{0n} are calculated for 415 ppm CO₂ and the absorption coefficient is then scaled for path length in cm and partial pressure in atm. In Figs. 1 and 2 are also included a comparison to measurement data which have been visually interpreted from [2, Fig. 2] as indicated here with the blue rings. The blue dashdotted lines indicate the sum of isolated Lorentzian lines, the red solid lines the basic projection method (66) together with (68) and (69) and the dashed black lines the modified projection method (66) together with (61) and (67). Here, $\nu'_s = p\tilde{\nu}'_s$ and the parameter $\tilde{\nu}'_s$ is furthermore chosen as $\tilde{\nu}'_s = c\tilde{\nu}'_{s'}$ with $c = 1.005$ in order to fine tune the absorption for a better match in the far wing. The Figs. 2 and 3 illustrate that this can be done without affecting the accuracy close to the line centers.

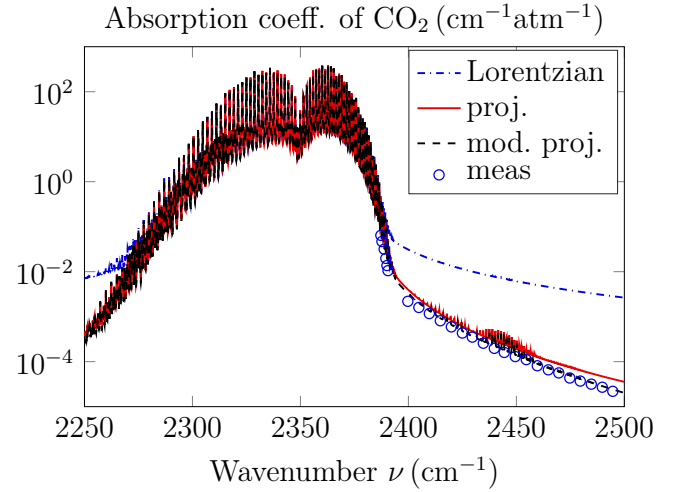


Fig. 1. Relative absorption coefficient for the ν_3 CO₂-band in dry air at $T = 20^\circ\text{C}$ and total pressure $p = 1$ atm calculated using HITRAN2016 parameters. The blue dashdotted line (Lorentzian) indicates the sum of isolated Lorentzian lines, the red solid line (proj.) the basic projection method and the dashed black line (mod. proj.) the modified projection method. The blue rings (meas) indicate the corresponding measurement data which have been visually interpreted from [2, Fig. 2].

VI. SUMMARY AND FUTURE RESEARCH

To summarize the present setting, we assume that we wish to express the spectral function $\tilde{C}(\omega)$ based on a diagonalization of the line mixing problem implemented as the following sum over individual lines

$$\tilde{C}(\omega) = \sum_n \frac{a_n^2 D_n(\omega)}{1 - \beta D_n(\omega)}, \quad (71)$$

where β is a Dicke narrowing parameter and a_n a complex valued constant as was derived in (22) and (23), cf., also [23,

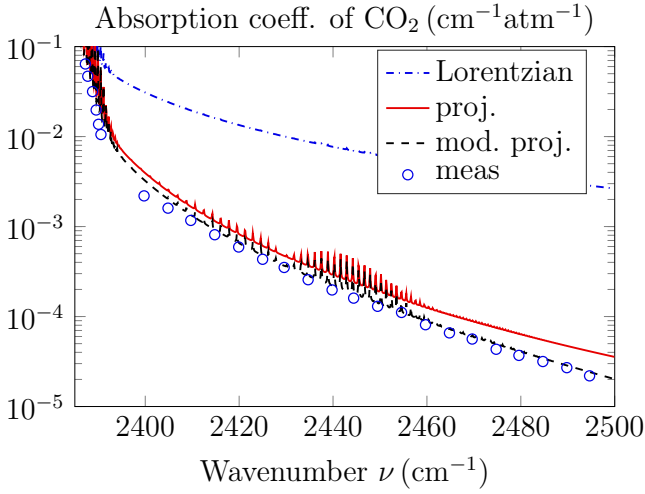


Fig. 2. Same plot as in Fig. 1 focusing on the wavenumber range 2385-2500 cm^{-1} . Notice how the modified projection (black dashed line) is able to improve the prediction of the basic projection method (red solid line) in the far wing region.

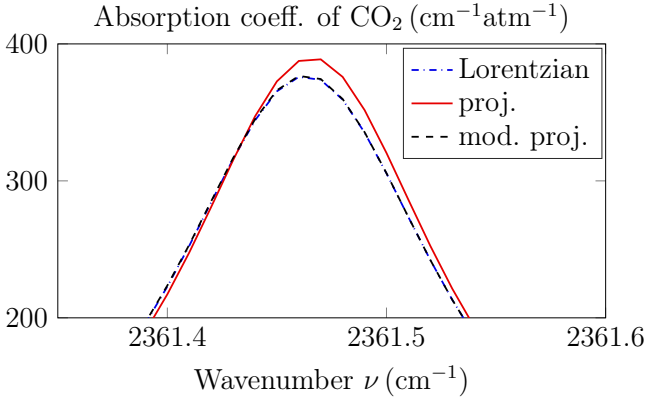


Fig. 3. Same plot as in Fig. 1 focusing on the wavenumber range 2361.35-2361.60 cm^{-1} , close to one of the ro-vibrational line centers. Notice how the modified projection (black dashed line) is able to improve the prediction of the basic projection method (red solid line) close to resonance. The modified projection is coincident with the isolated Lorentzian in this plot.

p. 381]. We have also from (20)

$$\begin{aligned}
 D_n(\omega) &= \int_{\mathbf{v}} \frac{f(\mathbf{v}) d\mathbf{v}}{\gamma_n + \beta - i(\omega - \omega_n) + i\mathbf{k} \cdot \mathbf{v}} \\
 &= \frac{\sqrt{\pi}}{k\tilde{v}} w\left(\frac{\omega - \omega_n + i(\gamma_n + \beta)}{k\tilde{v}}\right) \sim \frac{1}{\gamma_n + \beta - i(\omega - \omega_n)} \quad (72)
 \end{aligned}$$

where the second equality is valid when the eigenvalues of the relaxation matrix $\lambda_n = \gamma_n + i\omega_n$ are independent of velocity and the last expression is the asymptotic limit when the wavenumber k approaches zero (in which case β becomes redundant). Here, $w(\cdot)$ denotes the Faddeeva function.

The modified projection method is defined by (33) and (36) where $\gamma_{0n}(v)$ and $\delta_{0n}(v)$ are any high resolution isolated line broadening and shift parameters of interest that may or may not depend on speed v . The parameter $v_s = cv_s^{\text{ls}}$ quantifies the strength of the line coupling transfer rates where v_s^{ls} is

given by (36). The parameter c is very close to one and can be used to fine tune the far wing absorption to match any given measurement data. An exact solution for the static case (setting $k = 0$ means pure pressure broadening) and with velocity independent parameters is given by (50) and (51).

The first order Rosenkranz parameters for the modified projection method are given by (37) and (38) where p is pressure and $v_s = p\hat{v}_s$, etc. The eigenvalue parameters are $\gamma_n(v) = p\hat{\gamma}_{0n}(v)$ and $\omega_n(v) = \omega_{0n} + p\hat{\delta}_{0n}(v)$ where ω_{0n} are the molecular transition frequencies. The parameter a_n given by (38) is determined solely by the design parameter c together with the center frequencies ω_{0n} , the line widths γ_{0n} and the line strengths S_n which are readily available in spectroscopic databases such as *e.g.*, HITRAN [11]–[15].

The following research topics of interest can now be foreseen.

A. Validation of the modified projection method using measured spectroscopic data

The exact solution (50) and (51) for the static case with pressure broadening will be further validated against measured spectroscopic data for other species and frequency bands, similar as in Figs. 1 through 3. We will also validate the accuracy of the modified projection method in the case when Doppler broadening is present and the Rosenkranz approximation is incorporated in the implementation of the line mixing parameters as explained above. In the case with velocity independent broadening and shift parameters γ_{0n} and δ_{0n} , the Doppler effect can be incorporated by considering the second equality in (72) where $w(\cdot)$ is the Faddeeva function. The investigation is aiming to explore our hypothesis that a high model accuracy can be maintained close to the line centers at the same time as the absorption in the far wing can be fine tuned to reach the required accuracy for various species and frequency bands.

B. Efficient computation for Doppler broadening

There are many efficient numerical codes developed for the implementation of the Faddeeva function, see *e.g.*, [20], [35]–[38]. However, for computationally exhaustive broadband line by line analysis of radiative transfer in the atmosphere, the numerical evaluation of the Faddeeva function is still a bottleneck. It is much more efficient just to compute its asymptotic limit when this is appropriate, *i.e.*, at higher pressure when γ_{0n} is relatively large and in the far wing regions where $\omega - \omega_{0n}$ is relatively large. It has been proven in [10] that the Voigt profile converges uniformly to the Lorentzian on the whole of its domain as $\gamma_{0n}/k\tilde{v} \rightarrow \infty$. It has furthermore been proven that the Voigt profile converges uniformly to the Lorentzian as $(\omega - \omega_{0n})/k\tilde{v} \rightarrow \infty$. Based on these theoretical assertions, it is safe to employ numerical means to determine the corresponding criteria for achieving rigorous error bounds, *cf.*, [10]. However, the corresponding bounds have not yet been established in the case of line mixing as in (71). This investigation is therefore aiming to develop rigorous and readily implementable criteria for applying the last line in

(72) in terms of the given ratios $(\omega - \omega_{0n})/k\tilde{v}$, $(\gamma_{0n} + \beta)/k\tilde{v}$ as well as the line mixing parameter a_n .

C. Extension to velocity dependent parameters

It has been reported that the highly accurate Hartmann-Tran (HT) line shapes can take line mixing effects into account by simple empirical modifications, *cf.*, *e.g.*, [19, Eq. (9)] and [30, Eq. (15)]. However, it is not clear how accurate these modifications are with respect to the far wing absorption. The Hartmann-Tran profile is based on the following quadratic model for the speed-dependent pressure broadening and shifts

$$\gamma_{0n}(v) + i\delta_{0n}(v) = C_{0n} + C_{2n}(v^2/\tilde{v}^2 - 3/2) \quad (73)$$

where

$$\begin{cases} C_{0n} = \gamma_{0n} + i\delta_{0n}, \\ C_{2n} = \gamma_{2n} + i\delta_{2n}, \end{cases} \quad (74)$$

and where it is noted that $\langle v^2/\tilde{v}^2 \rangle = \int_{\mathbf{v}} f(\mathbf{v})(v^2/\tilde{v}^2) d\mathbf{v} = 3/2$. This quadratic model is now amenable for an analytic solution in the framework of the proposed modified projection method under the Rosenkranz approximation as described above. In particular, the defining integral in (72) becomes

$$\begin{aligned} D_n(\omega) &= \int_{\mathbf{v}} \frac{f(\mathbf{v})d\mathbf{v}}{\gamma_n + \beta - i(\omega - \omega_n) + i\mathbf{k} \cdot \mathbf{v}} \\ &= \int_{\mathbf{v}} \frac{f(\mathbf{v})d\mathbf{v}}{C_{0n} + C_{2n}(v^2/\tilde{v}^2 - 3/2) + \beta - i(\omega - \omega_n) + i\mathbf{k} \cdot \mathbf{v}}, \end{aligned} \quad (75)$$

and which can be expressed explicitly in terms of two Faddeeva function evaluations as explained in [19, Appendix A and B]. The distinguishing feature of the proposed modified projection method is then the way in which the Rosenkranz parameter a_n is calculated with an option to fine tune the parameter $v_s = cv_s^{\text{ls}}$ for a better far wing accuracy as described above.

It should be noted that the isolated HT profile in general is able to handle partially correlated collisions. However, following [23], it turns out that a rigorous diagonalization of the line mixing problem as in (71) can only be achieved with uncorrelated collisions, line independent Dicke narrowing and speed independent pressure broadening and shifts, see in particular [23, Appendix A]. On the other hand, by relaxing the statement above we can readily see that within the first order Rosenkranz approximation it is in fact possible to achieve a rigorous diagonalization including speed dependent parameters and with an option to efficiently fine tune the absorption in the far wing. This investigation is aiming to explore and validate the HT line mixing method as well as the proposed projection based method in these regards, based on theory as well as on experimental spectroscopic data.

D. Positivity of the spectral function

From a quantum mechanical point of view, it can readily be seen that dipole autocorrelation function $C(t)$ is positive definite and hence that it follows from Bochner's theorem that its Fourier transform $I(\omega)$ must be a positive measure,

cf., [39, p. 13]. However, from the point of view of the general Boltzmann-Liouville transport equation (1), it is not at all clear what the conditions are for producing a positive spectral density function. There are of course related criteria available in the literature concerning state space equations such as the positive real lemma [40]. However, these are not readily applicable in the present context where we have an integro-differential equation involving velocity space and complex valued parameters.

Virtually all spectroscopic models of today involve the Faddeeva function $w(z)$, *cf.*, *e.g.*, [19], [20], [38]. The Faddeeva function itself is indeed a positive real function as $\text{Re}\{w(is)\} > 0$ for $\text{Re}\{s\} > 0$, see *e.g.*, [41, Eq. 7.1.4]. However, it is not at all clear what the conditions are for spectroscopic parameters to produce a positive real function $\tilde{C}(\omega)$ in complicated scenarios such as with the partially Correlated quadratic-Speed-Dependent Hard-Collision profile (pCqSD-HCP), also known as the Hartmann-Tran Profile (HTP) [20]. For all practical purposes, both the HTP as well as the basic projection based strong collision (SC) method [2] will produce positive spectra as long as all the related parameters have sound physical meaning and are appropriately chosen to match experimental data of high quality. However, we can readily see that the proposed modified projection method (33) which is based on a perturbation may easily produce an indefinite spectral density $I(\omega)$ if the strength of the line coupling transfer rates v_s is chosen too large in relation to the given diagonal elements. In fact, based on our experience, it seems that optimal values for v_s may be very close to the point where $I(\omega)$ becomes indefinite. This is a very interesting and important observation. This investigation is therefore aiming to explore this topic in the framework of analytic function theory, passive systems and Herglotz (or positive real) functions [42]. What exactly are the conditions on the line mixing parameters in (1) to produce positive definite spectra? How can we understand this from a physical/mathematical point of view?

APPENDIX

A. Integrals involving the Faddeeva function

Some of the important integral relationships involving the Maxwell-Boltzmann distribution as well as the Faddeeva function used in this paper are summarized below. The Faddeeva function is an entire function defined by $w(z) = e^{-z^2} \text{erfc}(-iz)$ where $\text{erfc}(z)$ is the complementary error function defined by $\text{erfc}(z) = \frac{2}{\sqrt{\pi}} \int_z^\infty e^{-t^2} dt$, see *e.g.*, [43, Eq. (7.2.1)–(7.2.3)]. The Faddeeva function is of fundamental importance and very convenient to use in spectroscopic modeling due to the vast literature that is available on the theory, algorithms and computer codes for its efficient numerical evaluation, see *e.g.*, [20], [35]–[38]. The Maxwell-Boltzmann velocity distribution is given by $f(\mathbf{v}) = (\sqrt{\pi}\tilde{v})^{-3} e^{-(v/\tilde{v})^2}$ where $v = |\mathbf{v}|$, $\tilde{v} = \sqrt{2k_B T/\mu_r}$ is the most probable speed, k_B the Boltzmann constant, T the temperature and μ_r the mass of the radiator, *cf.*, [44, Chapt. 5].

The first integral of interest here is the standard result

$$\int_{\mathbf{v}} f(\mathbf{v}) e^{-i\mathbf{k}\cdot\mathbf{v}t} d\mathbf{v} = e^{-(k\tilde{v}t/2)^2}, \quad (76)$$

where $\mathbf{k} = k\hat{\mathbf{k}}$ is the wave vector associated with the incident radiation, see e.g., [16]. The integral identity (76) can readily be obtained by a substitution to spherical coordinates and is valid for all $t \in \mathbb{R}$.

By completing the squares in the exponent and employing the definition of the complementary error function, one can also derive the following Fourier-Laplace transform

$$\int_0^\infty e^{-(k\tilde{v}t/2)^2} e^{i\omega t} dt = \frac{\sqrt{\pi}}{k\tilde{v}} w\left(\frac{\omega}{k\tilde{v}}\right), \quad (77)$$

which is valid for all $\omega \in \mathbb{C}$. Another useful integral identity can also be derived by inserting the result (76) into (77) and changing the order of integration to yield

$$\int_{\mathbf{v}} \frac{f(\mathbf{v}) d\mathbf{v}}{i\mathbf{k}\cdot\mathbf{v} - i\omega} = \frac{\sqrt{\pi}}{k\tilde{v}} w\left(\frac{\omega}{k\tilde{v}}\right), \quad (78)$$

but which is now valid only for $\text{Im}\{\omega\} > 0$. The latter restriction is usually not a problem since the resulting right-hand side can be analytically extended to the whole complex plane. An important example is the relation $\frac{1}{\pi} \text{Re} \left\{ \frac{\sqrt{\pi}}{k\tilde{v}} w\left(\frac{\omega}{k\tilde{v}}\right) \right\} = \frac{1}{\sqrt{\pi k\tilde{v}}} e^{-\omega^2/k^2\tilde{v}^2}$ where $\omega \in \mathbb{R}$, and which is a well known formula for Doppler broadening, cf., e.g., [3], [16], [20]. The integral identities (76), (77) and (78) are standard integrals which are employed in many papers, such as e.g., [19], [23].

REFERENCES

- [1] N. N. Filippov, V. P. Ogibalov, and M. V. Tonkov, "Line mixing effect on the pure CO₂ absorption in the 15 μm region," *Journal of Quantitative Spectroscopy & Radiative Transfer*, vol. 72, pp. 315–325, 2002.
- [2] M. V. Tonkov and N. N. Filippov, "Collision Induced Far Wings of CO₂ and H₂O Bands in IR Spectra," *Camy-Peyret C., Viganin A.A. (eds) Weakly Interacting Molecular Pairs: Unconventional Absorbers of Radiation in the Atmosphere. NATO Science Series (Series IV: Earth and Environmental Sciences)*, vol. 27, pp. 125–136, 2003.
- [3] J.-M. Hartmann, C. Boulet, and D. Robert, *Collisional effects on molecular spectra. Laboratory experiments and models, consequences for applications*. Amsterdam: Elsevier, 2008.
- [4] A. B. Dokuchaev, N. N. Filippov, and M. V. Tonkov, "Line interference in ν₃ rotational-vibrational band of N₂O in the strong interaction approximation," *Physica Scripta*, vol. 25, pp. 378–380, 1982.
- [5] M. O. Bulanin, A. B. Dokuchaev, M. V. Tonkov, and N. N. Filippov, "Influence of line interference on the vibration-rotation band shapes," *Journal of Quantitative Spectroscopy & Radiative Transfer*, vol. 31, no. 6, pp. 521–543, 1984.
- [6] N. N. Filippov and M. V. Tonkov, "Semiclassical analysis of line mixing in the infrared bands of CO and CO₂," *Journal of Quantitative Spectroscopy & Radiative Transfer*, vol. 50, no. 1, pp. 111–125, 1993.
- [7] M. V. Tonkov, N. N. Filippov, Y. M. Timofeyev, and A. V. Polyakov, "A simple model of the line mixing effect for atmospheric applications: Theoretical background and comparison with experimental profiles," *Journal of Quantitative Spectroscopy & Radiative Transfer*, vol. 56, no. 5, pp. 783–795, 1996.
- [8] K. N. Liou, *An introduction to atmospheric radiation*. London, UK: Academic Press, 2002.
- [9] A. Berk and F. Hawes, "Validation of MODTRAN 6 and its line-by-line algorithm," *Journal of Quantitative Spectroscopy & Radiative Transfer*, vol. 203, pp. 542–556, 2017.
- [10] S. Nordebo, "Uniform error bounds for fast calculation of approximate Voigt profiles," *Journal of Quantitative Spectroscopy & Radiative Transfer*, vol. 270, p. 107715, 2021.
- [11] "HITRANOnline. The HITRAN Database. <https://hitran.org>."
- [12] "HITRANOnline. Definitions and units: Line-by-line parameters. <https://hitran.org/docs/definitions-and-units/>."
- [13] L. S. Rothman and et al, "The HITRAN molecular spectroscopic database and HAWKS (HITRAN atmospheric workstation): 1996 edition," *Journal of Quantitative Spectroscopy & Radiative Transfer*, vol. 60, no. 5, pp. 665–710, 1998.
- [14] M. Šimečková, D. Jacquemart, L. S. Rothman, R. R. Gamache, and A. Goldman, "Einstein A-coefficients and statistical weights for molecular absorption transitions in the HITRAN database," *Journal of Quantitative Spectroscopy & Radiative Transfer*, vol. 98, pp. 130–155, 2006.
- [15] I. E. Gordon, L. S. Rothman, C. Hill, R. V. Kochanov, Y. Tan, P. F. Bernath, M. Birk, V. Boudon, A. Campargue, K. V. Chance, B. J. Drouin, J.-M. Flaud, R. R. Gamache, J. T. Hodges, D. Jacquemart, V. I. Perevalov, A. Perrin, K. P. Shine, M.-A. H. Smith, J. Tennyson, G. C. Toon, H. Tran, V. G. Tyuterev, A. Barbe, A. G. Császár, V. M. Devi, J. J. H. T. Furtenbacher, J.-M. Hartmann, A. Jolly, T. J. Johnson, T. Karman, I. Kleiner, A. A. Kyuberis, J. Loos, O. M. Lyulin, S. T. Massie, S. N. Mikhailenko, N. Moazzen-Ahmadi, H. S. P. Müller, O. V. Naumenko, A. V. Nikitin, O. L. Polyansky, M. Rey, M. Rotger, S. W. Sharpe, K. Sung, E. Starikova, S. A. Tashkun, J. V. Auwera, G. Wagner, J. Wilzewski, P. Wcislo, S. Yu, and E. J. Zak, "The HITRAN2016 molecular spectroscopic database," *Journal of Quantitative Spectroscopy & Radiative Transfer*, vol. 203, pp. 3–69, 2017.
- [16] S. G. Rautian and I. I. Sobel'man, "The effect of collisions on the Doppler broadening of spectral lines," *Soviet Physics Uspekhi*, vol. 9, no. 5, pp. 701–716, 1967.
- [17] H. Tran and J.-M. Hartmann, "An isolated line-shape model based on the Keilson and Storer function for velocity changes. I. Theoretical approaches," *J. Chem. Phys.*, vol. 130, p. 094301, 2009.
- [18] N. H. Ngo, H. Tran, and R. R. Gamache, "A pure H₂O isolated line-shape model based on classical molecular dynamics simulations of velocity changes and semi-classical calculations of speed-dependent collisional parameters," *J. Chem. Phys.*, vol. 136, p. 154310, 2012.
- [19] N. Ngo, D. Lisak, H. Tran, and J.-M. Hartmann, "An isolated line-shape model to go beyond the Voigt profile in spectroscopic databases and radiative transfer codes," *Journal of Quantitative Spectroscopy & Radiative Transfer*, vol. 129, pp. 89–100, 2013.
- [20] J. Tennyson, P. F. Bernath, A. Campargue, A. G. Császár, L. Daumont, R. R. Gamache, J. T. Hodges, D. Lisak, O. V. Naumenko, L. S. Rothman, H. Tran, N. F. Zobov, J. Buldyreva, C. D. Boone, M. D. D. Vizia, L. Gianfrani, J.-M. Hartmann, R. McPheat, D. Weidmann, J. Murray, N. H. Ngo, and O. L. Polyansky, "Recommended isolated-line profile for representing high-resolution spectroscopic transitions (IUPAC Technical Report)," *Pure Appl. Chem.*, vol. 86, pp. 1931–1943, 2014.
- [21] E. W. Smith, J. Cooper, W. R. Chappell, and T. Dillon, "An impact theory for Doppler and pressure broadening. I. General theory," *Journal of Quantitative Spectroscopy & Radiative Transfer*, vol. 11, pp. 1547–1565, 1971.
- [22] —, "An impact theory for Doppler and pressure broadening. II. Atomic and molecular systems," *Journal of Quantitative Spectroscopy & Radiative Transfer*, vol. 11, pp. 1567–1576, 1971.
- [23] R. Ciuryło and A. S. Pine, "Speed-dependent line mixing profiles," *Journal of Quantitative Spectroscopy & Radiative Transfer*, vol. 67, pp. 375–393, 2000.
- [24] A. C. Kolb and H. Griem, "Theory of line broadening in multiplet spectra," *Physical Review*, vol. 111, no. 2, pp. 514–521, 1958.
- [25] M. Baranger, "General impact theory of pressure broadening," *Physical Review*, vol. 112, no. 3, pp. 855–865, 1958.
- [26] R. G. Gordon, "Semiclassical theory of spectra and relaxation in molecular gases," *J. Chem. Phys.*, vol. 45, no. 5, pp. 1649–1655, 1966.
- [27] —, "On the pressure broadening of molecular multiplet spectra," *J. Chem. Phys.*, vol. 46, no. 2, pp. 448–455, 1967.
- [28] P. W. Rosenkrantz, "Shape of the 5 mm oxygen band in the atmosphere," *IEEE Trans. Antennas Propagat.*, vol. 23, no. 4, pp. 498–506, 1975.
- [29] I. E. Gordon and et al, "The HITRAN2020 molecular spectroscopic database," *Journal of Quantitative Spectroscopy & Radiative Transfer*, vol. 277, pp. 1–82, 2022.
- [30] A. S. Pine and T. Gabard, "Speed-dependent broadening and line mixing in CH₄ perturbed by Ar and N₂ from multispectrum fits," *Journal of Quantitative Spectroscopy & Radiative Transfer*, vol. 66, pp. 69–92, 2000.
- [31] R. G. Gordon, "Theory of the width and shift of molecular spectral lines in gases," *J. Chem. Phys.*, vol. 44, no. 8, pp. 3083–3089, 1966.

- [32] D. Robert and L. Galatry, "Infrared absorption of diatomic polar molecules in liquid solutions," *J. Chem. Phys.*, vol. 55, no. 5, pp. 2347–2359, 1971.
- [33] R. A. Horn and C. R. Johnson, *Matrix Analysis*. Cambridge University Press, 1985.
- [34] J. M. Mendel, *Lessons in digital estimation theory*. Englewood Cliffs, New Jersey: Prentice-Hall, Inc., 1987.
- [35] B. H. Armstrong, "Spectrum line profiles: The Voigt function," *Journal of Quantitative Spectroscopy & Radiative Transfer*, vol. 7, pp. 61–88, 1967.
- [36] F. Schreier, "The Voigt and complex error function: A comparison of computational methods," *Journal of Quantitative Spectroscopy & Radiative Transfer*, vol. 48, no. 5/6, pp. 743–762, 1992.
- [37] —, "Optimized implementations of rational approximations for the Voigt and complex error function," *Journal of Quantitative Spectroscopy & Radiative Transfer*, vol. 112, pp. 1010–1025, 2011.
- [38] S. M. Abrarov and B. M. Quine, "Efficient algorithmic implementation of the Voigt/complex error function based on exponential series approximation," *Appl. Math. Comput.*, vol. 218, pp. 1894–1902, 2011.
- [39] M. Reed and B. Simon, *Methods of modern mathematical physics*. New York: Academic Press, 1975, vol. II: Fourier analysis, Self-adjointness.
- [40] S. Boyd, L. Ghaoui, E. Feron, and V. Balakrishnan, *Linear Matrix Inequalities in System and Control Theory*. Philadelphia, PA: Society for Industrial and Applied Mathematics, 1994.
- [41] M. Abramowitz and I. A. Stegun, Eds., *Handbook of Mathematical Functions*, ser. Applied Mathematics Series No. 55. Washington D.C.: National Bureau of Standards, 1970.
- [42] M. Nedic, C. Ehrenborg, Y. Ivanenko, A. Ludvig-Osipov, S. Nordebo, A. Luger, B. L. G. Jonsson, D. Sjöberg, and M. Gustafsson, *Herglotz functions and applications in electromagnetics*. IET, 2019, editor: K. Kobayashi and P. Smith.
- [43] F. W. J. Olver, D. W. Lozier, R. F. Boisvert, and C. W. Clark, *NIST Handbook of mathematical functions*. New York: Cambridge University Press, 2010.
- [44] S. J. Blundell and K. M. Blundell, *Concepts in thermal physics*. New York: Oxford University Press Inc., 2010.